Petrophysical seismic inversion conditioned to well-log data: Methods and application to a gas reservoir

Miguel Bosch¹, Carla Carvajal², Juan Rodrigues¹, Astrid Torres², Milagrosa Aldana³, and Jesús Sierra⁴

ABSTRACT

Hydrocarbon reservoirs are characterized by seismic, well-log, and petrophysical information, which is dissimilar in spatial distribution, scale, and relationship to reservoir properties. We combine this diverse information in a unified inverse-problem formulation using a multiproperty, multiscale model, linking properties statistically by petrophysical relationships and conditioning them to well-log data. Two approaches help us: (1) Markov-chain Monte Carlo sampling, which generates many reservoir realizations for estimating medium properties and posterior marginal probabilities, and (2) optimization with a least-squares iterative technique to obtain the most probable model configuration. Our petrophysical model, applied to near-vertical-anglestacked

seismic data and well-log data from a gas reservoir, includes a deterministic component, based on a combination of Wyllie and Wood relationships calibrated with the well-log data, and a random component, based on the statistical characterization of the deviations of well-log data from the petrophysical transform. At the petrophysical level, the effects of porosity and saturation on acoustic impedance are coupled; conditioning the inversion to well-log data helps resolve this ambiguity. The combination of well logs, petrophysics, and seismic inversion builds on the corresponding strengths of each type of information, jointly improving (1) cross resolution of reservoir properties, (2) vertical resolution of property fields, (3) compliance to the smooth trend of property fields, and (4) agreement with well-log data at well positions.

INTRODUCTION

The 3D characterization of hydrocarbon reservoirs requires integrating information across medium properties at different spatial scales and distributions: (1) high-resolution well-log information at irregularly distributed well paths, (2) uniformly sampled information from 3D seismic data with low vertical resolution, (3) petrophysical information relating reservoir properties and scales, and (4) geostatistical information relating property fields in space. Common procedures rely on stepwise processing of the different types of data and information (seismic, well log, petrophysical, and geostatistical) and their combination in various work flows. The goal of our work is to describe a method to integrate this information into a unified inversion scheme, accounting for nonlinear relations across me-

dium properties and data as well as the combination of uncertainties related to the various information components.

The combination of well-log data and seismic information for estimating reservoir and elastic medium properties has motivated the development of different techniques. In Doyen (1988), well-log porosities are extrapolated by correlation with the acoustic impedance estimated from seismic data, using the well-known cokriging technique. An additional step in integrating seismic data within geostatistical methods is described by Haas and Dubrule (1994), who propose a method to generate acoustic impedance realizations conditioned to the well-log data and seismic stacked data simulated by 1D convolution of the model reflectivity. Also, Torres-Verdin et al. (1999) focus on the problem of generating realizations of acoustic impedance and discrete facies types jointly honoring stacked seis-

Manuscript received by the Editor 5 March 2008; revised manuscript received 17 September 2008; published online 4 February 2009.

¹Universidad Central of Venezuela, Geophysical Simulation and Inversion Laboratory, Engineering Faculty, Caracas, Venezuela. E-mail: miguel.bosch@ucv.ve.

²Universidad Central of Venezuela, Geophysical Simulation and Inversion Laboratory, and Universidad Simón Bolivar, Department of Earth Sciences, Caracas Venezuela

cas, Venezuela. Universidad Simón Bolivar, Department of Earth Sciences, Caracas, Venezuela. E-mail: maldana@usb.ve.

⁴IGS Services and Consulting, Caracas, Venezuela. E-mail: jesus.sierra@igs-sc.com.

^{© 2009} Society of Exploration Geophysicists. All rights reserved.

O2 Bosch et al.

mic data and well logs using a simulated annealing technique. Integration of well-log data and seismic data partially stacked at different incidence angle ranges is described by Contreras et al. (2005) for joint estimation of elastic medium parameters and facies types. In Gonzalez et al. (2008), facies types also are related with seismic data using a multipoint geostatistical model that honors spatial well constraints.

We can circumscribe these works to the field of *geostatistical* inversion of seismic data. The advantages of geostatistical inversion related to plain geophysical inversion are manifold: estimated property fields match well-log data at well location, seismic data are honored, and field resolution increases along the well direction in the region within the range of spatial property correlation.

Effort has been directed to integrate petrophysical and geophysical inversion within a common inference formulation. In this approach, the seismic data are inverted under the constraint of a petrophysical model and prior information; the result is a joint estimate of elastic and reservoir (e.g., porosity, facies, fluid) properties. In Bosch (2004), a statistical formulation for the joint inversion is described and numerical examples are presented for the case of inverting short-offset seismic data to estimate acoustic impedance and porosity. The relation between impedance and porosity is embodied in a petrophysical mixed model (deterministic mean and random deviations) calibrated to well-log data; an optimization method is used to produce a linear system of equations for the joint porosity and impedance model updates. Bosch et al. (2007) describe a similar formulation to solve the inference problem with a sampling Monte Carlo approach, providing an application to a field case. Also, Spikes et al. (2007) focus on constraining a seismic inversion with a petrophysical model calibrated to well-log data and estimating elastic and reservoir parameters from two constant-angle stacks, showing a field case. Larsen et al. (2006), Buland and Omre (2006), and Gunning and Glinski (2007) describe similar methods illustrated by synthetic tests.

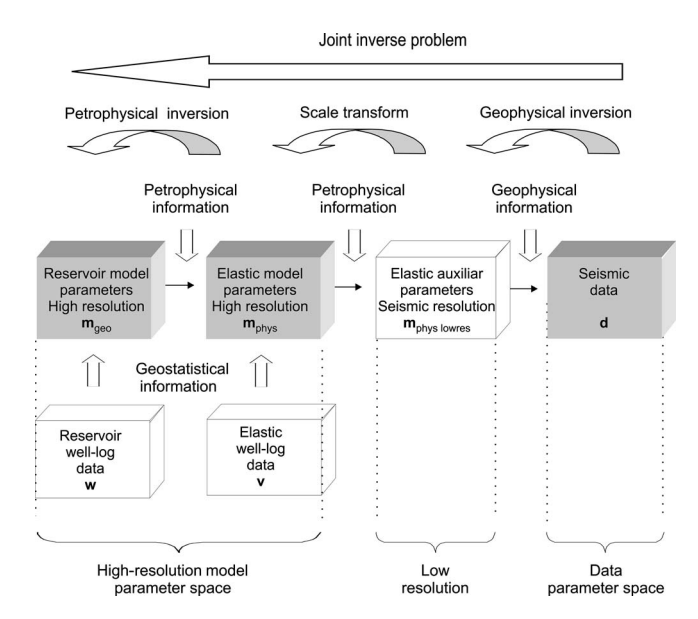


Figure 1. Model parameters and data involved in the inference problem—information components and their relations. Thin black arrows indicate the forward-modeling sense. Thick arrows indicate the inverse sense.

We can group these works in the field of *petrophysical* inversion of seismic data. The advantages of petrophysical inversion compared to plain seismic inversion are also manifold: reservoir properties are estimated in addition to elastic properties, relations across medium properties honor the petrophysical model, and prior information constraining the reservoir properties holds. Other ways to combine seismic and petrophysical information follow a two-step process: (1) calculating seismic attributes or inverting the seismic data and (2) using these results within a petrophysical statistical model to estimate reservoir parameters. Work by Eidsvik et al. (2004), Bachrach (2006), Mukerji et al. (2001), Saltzer et al. (2005), and Sengupta and Bachrach (2007) is based on this approach.

Our work extends the method of petrophysical inversion described by Bosch (2004) and Bosch et al. (2007) to include well-log data constrained on the basis of a geostatistical model, combining benefits of the geostatistical and petrophysical approaches and integrating surface seismic data, well-log data, petrophysics, and geostatistics. We parameterize the model in two scales to address the different resolution of well logs and seismic data, with a scale relation between them based on petrophysical change of support transforms. Effective medium theory (Backus, 1962; Schoenberg and Muir, 1989) describes averaging functions to obtain the elastic medium parameters at seismic resolution from the corresponding parameters at finer resolution; it also encompasses the full anisotropic elastic stiffness tensor parameters. Impedances, for instance, commonly are lower at seismic scale than the corresponding impedances measured at well-log scale. Ray theory, on the other hand, provides averaging functions for the properties, assuming high-frequency propagation.

The two formulations correspond to the upper and lower limits of the ratio between the wavelength and the characteristic thickness of the strata. Behavior at intermediate ratios is bounded approximately by the effective media and ray-theory results, depending on factors such as the statistical spatial characterization of the heterogeneities and the actual frequency composition of the signal as shown by modeling and laboratory tests (Mukerji, 1995; Grechka, 2003; Stovas and Arntsen, 2006). In many practical applications to reservoirs, an intermediate recipe combining the two bounds is recommended (Rio et al., 1996). Here, we use an upscaling formulation of the impedance that lies between these two limits.

We describe our methods, characterize the well-log data to calibrate our petrophysical and geostatistical models, and apply two different inversion techniques — sampling and optimization — to seismic data from a gas reservoir area. For comparison, we show the results obtained from the seismic petrophysical inversion with no well conditioning, the plain geostatistical estimation, and the seismic inversion conditioned by the well-log data.

THEORY AND METHOD

The joint model parameter array is a composition, $\mathbf{m} = (\mathbf{m}_{\rm geo}, \mathbf{m}_{\rm elas})$, of parameters describing the reservoir property fields $\mathbf{m}_{\rm geo}$ and parameters describing the elastic-property fields $\mathbf{m}_{\rm elas}$. In addition, the elastic properties are described at two different vertical scales: (1) high-resolution parameters linked with the well-log information and (2) low-resolution parameters according to the vertical resolution of the seismic data. Figure 1 describes the model parameters, the data subspaces, the information involved in the problem, and their relations.

Statistical formulation

The knowledge about medium parameters is described with a probability density function (PDF) that combines the different types of information and data considered. The combined probability density is given by the product of three factors that cast the types of information included in our problem (Bosch, 1999):

$$\sigma(\mathbf{m}_{\rm elas}, \mathbf{m}_{\rm geo}) = c \underbrace{L_{\rm seis}(\mathbf{m}_{\rm elas})}_{\rm geophysics} \underbrace{\pi(\mathbf{m}_{\rm elas}|\mathbf{m}_{\rm geo})}_{\rm petrophysics} \underbrace{\rho_{\rm geo}(\mathbf{m}_{\rm geo})}_{\rm geostatistics}. \tag{1}$$

The PDF $\rho_{\rm gco}(\mathbf{m}_{\rm gco})$ describes the prior geostatistical information in the reservoir property fields, including the well-data constraints. The conditional probability density $\pi(\mathbf{m}_{\rm elas}|\mathbf{m}_{\rm gco})$ is a petrophysical likelihood function, based on the petrophysical model that predicts the elastic properties from the reservoir properties. In addition, this factor embodies geostatistical constraints of the elastic properties; it measures the probability of the elastic-property fields given a particular reservoir field configuration and well-log measurements. The factor $L_{\rm seis}(\mathbf{m}_{\rm elas})$ is the geophysical likelihood function that measures the proximity between the observed and calculated seismic data. It depends on the elastic-property field parameters. We model each of the factors of the combined probability density with multivariate parametric functions and implement solution methods by sampling and optimization approaches.

As common in geostatistical formulation, property fields are modeled as a multidimensional random variable, with components being the values of the properties at a given set of points in the medium volume. We model the reservoir-property fields, prior to the well-log constraints, with a Gaussian multivariate prior probability density. Conditioning the Gaussian property field to known values of correlated properties at a given set of points (here, the well-log estimates of the property field) results in a random Gaussian field with probability density

$$\rho_{\text{geo}}(\mathbf{m}_{\text{geo}}) = c_2 \exp[-1/2(\mathbf{m}_{\text{geo}} - \mathbf{m}_{\text{geo krig}})^{\text{T}} \times \mathbf{C}_{\text{geo krig}}^{-1}(\mathbf{m}_{\text{geo}} - \mathbf{m}_{\text{geo krig}})],$$
(2)

where $\mathbf{m}_{\text{geo krig}}$ and $\mathbf{C}_{\text{geo krig}}$ are the simple cokriging estimate and covariance that result from the geostatistical interpolation of the well-log data. For a review on geostatistical estimation and conditional simulation, see Isaaks and Srivastava (1989), Chiles and Delfiner (1999), and Dubrule (2003).

In our model, the elastic-medium properties depend on the reservoir properties. To describe their relationship, we use a mixed model superimposing a deterministic petrophysical transform $f(m_{\rm geo})$ for the central trend and random deviations from the transform $m_{\rm elas} = f(m_{\rm geo}) + m_{\rm dev}$. We also call petrophysical misfits the deviations $m_{\rm dev}$ of the elastic properties from the corresponding prediction of the petrophysical transform of the reservoir parameters. Before constraining the property field with the well-log measurements, we model the petrophysical misfits with a multivariate Gaussian probability density. Parameters of the Gaussian density, such as the covariance function, can be characterized and modeled from the well-log data.

To condition the elastic parameters to the well-log observations, we constrain the elastic parameter deviations from the petrophysical transform to the corresponding deviations at the well points. The

constraint field is also Gaussian and is given by the probability density:

$$\varphi(\mathbf{m}_{\text{dev}}) = \exp[-1/2(\mathbf{m}_{\text{dev}} - \mathbf{m}_{\text{dev krig}})^{\text{T}} \times \mathbf{C}_{\text{dev krig}}^{-1}(\mathbf{m}_{\text{dev}} - \mathbf{m}_{\text{dev krig}})],$$
(3)

with $\mathbf{m}_{\text{dev krig}}$ and $\mathbf{m}_{\text{dev krig}}$ the simple cokriging estimate and covariance for the elastic-property deviations from the petrophysical transform. By substituting the petrophysical deviations $\mathbf{m}_{\text{dev}} = \mathbf{m}_{\text{elas}} - \mathbf{f}(\mathbf{m}_{\text{geo}})$ in equation 3, we have the expression for the petrophysical likelihood term constrained to the well-log measurements:

$$\pi(\mathbf{m}_{\text{elas}}|\mathbf{m}_{\text{geo}}) = \exp[-1/2(\mathbf{m}_{\text{elas}} - \mathbf{f}(\mathbf{m}_{\text{geo}}) - \mathbf{m}_{\text{dev krig}})^{\text{T}} \mathbf{C}_{\text{dev krig}}^{-1}(\mathbf{m}_{\text{elas}} - \mathbf{f}(\mathbf{m}_{\text{geo}}) - \mathbf{m}_{\text{dev krig}})].$$
(4)

The function provides a large likelihood for the model configurations that jointly honor well-log and petrophysical information.

The third factor in the combined probability density (equation 1) is a seismic likelihood. It is defined as a Gaussian function of the deviations of the observed seismic data \mathbf{d}_{obs} and the seismic data calculated from the model configuration \mathbf{d}_{cal} . The latter depends on the function that simulates the seismic response of the model $\mathbf{d}_{\text{cal}} = \mathbf{g}(\mathbf{m}_{\text{elas}}, \mathbf{m}_{\text{sou}})$, commonly a nonlinear function. Thus, we model the geophysical likelihood with the expression

$$L(\mathbf{m}_{\text{elas}}) = \exp[-1/2(\mathbf{g}(\mathbf{m}_{\text{elas}}) - \mathbf{d}_{\text{obs}})^{\text{T}} \times \mathbf{C}_{\text{dat}}^{-1}(\mathbf{g}(\mathbf{m}_{\text{elas}}) - \mathbf{d}_{\text{obs}})],$$
(5)

with C_{dat} being the data covariance matrix. In our particular case, the function $\mathbf{g}(\mathbf{m}_{\text{elas}})$ involves a scale transformation. It is the concatenation of two functions: $\mathbf{g}_{\text{scale}}(\mathbf{m}_{\text{elas}}) = \mathbf{m}_{\text{elas lowres}}$ for upscaling the elastic property model parameter from the high-resolution model to the low-resolution model (at seismic scale) and the forward function calculating the seismic data, $\mathbf{g}_{\text{scis}}(\mathbf{m}_{\text{elas lowres}}) = \mathbf{d}_{\text{cal}}$.

Modeling the geophysical likelihood by equation 5, the petrophysical likelihood by equation 4, and the prior probability density on the reservoir parameters by equation 2 fully defines the combined probability in equation 1. The combined probability depends on the seismic observed data, functions $f(\mathbf{m}_{geo})$ and $g(\mathbf{m}_{elas})$, solving the deterministic petrophysical and geophysical forward problems correspondingly—the well data from the cokriging estimates and covariances of the reservoir fields and the petrophysical deviation field, and reservoir data from prior densities.

Different strategies can be adopted to produce model configurations describing the information summarized by the combined probability density of equation 1; two major approaches are optimization and sampling. The first searches for a model configuration that maximizes the combined PDF; the second explores the model space producing a large set of joint model (reservoir elastic properties) realizations in proportion to the combined probability.

Probability estimation by Monte Carlo sampling

Following the sampling approach, we implement a Markov-chain algorithm adapted to the relation between parameters and the specific structure of the posterior probability density in equation 1, combining multivariate Gaussian, Gibbs, and Metropolis sampling techniques. Given a current model configuration, the next configuration

O4 Bosch et al.

in the chain is generated in the following manner:

- A set of parameters of the reservoir model is modified to generate a candidate Gaussian multivariate realization following the prior probability density for the reservoir parameters in expression 2. The candidate configuration is a realization of the cokriging probability density, honoring the well-log constraints on the reservoir properties.
- Sampling is extended to the elastic parameter space by evaluating the deterministic petrophysical transform and adding random multivariate Gaussian realizations of the petrophysical misfit.
- 3) The geophysical likelihood of the candidate realization is calculated by upscaling the elastic-property fields, computing the reflection coefficients, convolving the reflectivity series with the source function, and comparing the predicted seismic amplitudes with the observed amplitudes at the corresponding common depth point (CDP), as in equation 5.
- 4) The Metropolis rule is used to accept or reject the candidate model realization according to the likelihood ratio with the current realization in the chain. The acceptance probability is given by

$$p = \min[1, L(\mathbf{m}_{cand})/L(\mathbf{m}_n)], \tag{6}$$

where \mathbf{m}_{cand} is the candidate configuration and \mathbf{m}_n is the current model configuration. When the candidate model configuration is rejected, the current model stands for the next step in the sampling chain, $\mathbf{m}_{n+1} = \mathbf{m}_n$.

The process repeats for the next step of the chain and iterates; the procedure warrants convergence of the chain to the combined probability density in equation 1. Hastings (1970), Geyer (1992), Smith and Roberts (1993), Tierney (1994), Mosegaard and Tarantola (1995), Bosch (1999), and Bosch et al. (2007) provide additional information on Markov-chain Monte Carlo sampling methods.

Objective function and optimization

The optimization approach searches for a model configuration that maximizes the combined probability density. Substituting the different factors in the combined probability of equation 1 and grouping their exponents in the objective function $S = S_{\rm geo} + S_{\rm elas} + S_{\rm seis}$, with

$$S_{\text{geo}} = 1/2(\mathbf{m}_{\text{geo}} - \mathbf{m}_{\text{geo krig}})^{\text{T}} \mathbf{C}_{\text{geo krig}}^{-1}(\mathbf{m}_{\text{geo}} - \mathbf{m}_{\text{geo krig}}),$$
(7)

$$S_{\text{elas}} = 1/2(\mathbf{m}_{\text{elas}} - \mathbf{f}(\mathbf{m}_{\text{geo}}) - \mathbf{k}_{\text{dev krig}})^{\text{T}}$$

$$\times \mathbf{C}_{\text{dev krig}}^{-1}(\mathbf{m}_{\text{elas}} - \mathbf{f}(\mathbf{m}_{\text{geo}}) - \mathbf{m}_{\text{dev krig}})], \tag{8}$$

and

$$S_{\text{seis}} = 1/2(\mathbf{g}(\mathbf{m}_{\text{elas}}) - \mathbf{d}_{\text{obs}})^{\text{T}} \mathbf{C}_{\text{dat}}^{-1}(\mathbf{g}(\mathbf{m}_{\text{elas}}) - \mathbf{d}_{\text{obs}}), \qquad (9)$$

the combined probability density can be written in terms of the objective function as $\sigma(\mathbf{m}_{\text{clas}}, \mathbf{m}_{\text{geo}}) = c \exp[-S]$. A maximum of the probability density corresponds to a minimum of the joint objective function S. Therefore, the solution of the optimization problem consists of searching for the joint model configuration that minimizes the objective function, jointly satisfying the proximity between (a)

the reservoir model configuration and the reservoir-property estimates obtained from the geostatistical interpolation of the well-log data, (b) the petrophysical relationship residuals and corresponding residuals interpolated from the well-log data, and (c) the calculated and observed seismic data.

We use Newton's method to develop an iterative procedure for updating the joint model configuration (physical and reservoir parameters) to converge to a local minimum of the misfit function. Given a current joint model configuration \mathbf{m}_n at iteration step n, Newton's method requires solving a linear system of equations $\mathbf{A} \Delta \mathbf{m} = \mathbf{b}$ to obtain the model update $\Delta \mathbf{m} = \mathbf{m}_{n+1} - \mathbf{m}_n$, where \mathbf{A} is the curvature matrix of the objective function and \mathbf{b} is the steepest-descent direction:

$$\mathbf{A} = \begin{pmatrix} \mathbf{I} & \mathbf{C}_{\text{geo krig}} \mathbf{F}^{\text{T}} \mathbf{G}^{\text{T}} \mathbf{C}_{\text{dat}}^{-1} \mathbf{G} \\ \mathbf{0} & \mathbf{I} + (\mathbf{C}_{\text{dev krig}} + \mathbf{F} \mathbf{C}_{\text{geo krig}} \mathbf{F}^{\text{T}}) \mathbf{G}^{\text{T}} \mathbf{C}_{\text{dat}}^{-1} \mathbf{G} \end{pmatrix},$$
(10)

$$\Delta \mathbf{m} = \begin{pmatrix} \Delta \mathbf{m}_{\text{geo}} \\ \Delta \mathbf{m}_{\text{phys}} \end{pmatrix}, \tag{11}$$

$$\mathbf{b} = \begin{pmatrix} \mathbf{m}_{geo~krig} - \mathbf{m}_{geo} + \mathbf{C}_{geo~krig} \mathbf{F}^{T} \mathbf{G}^{T} \mathbf{C}_{dat}^{-1} (\mathbf{d}_{obs} - \mathbf{g}(\mathbf{m}_{phys})) \\ \mathbf{f}(\mathbf{m}_{geo}) - \mathbf{m}_{phys} + \mathbf{m}_{dev~krig} + \mathbf{F}(\mathbf{m}_{geo~krig} - \mathbf{m}_{geo}) \\ + (\mathbf{F} \mathbf{C}_{geo~krig} \mathbf{F}^{T} + \mathbf{C}_{dev~krig}) \mathbf{G}^{T} \mathbf{C}_{dat}^{-1} (\mathbf{d}_{obs} - \mathbf{g}(\mathbf{m}_{phys})) \end{pmatrix}.$$
(12)

In expressions 10 and 11, $\mathbf{G} = (\partial \mathbf{g}/\partial \mathbf{m}_{elas})$ and $\mathbf{F} = (\partial \mathbf{f}/\partial \mathbf{m}_{geo})$ are the Jacobian matrices of $\mathbf{g}(\mathbf{m}_{elas})$ and $\mathbf{f}(\mathbf{m}_{geo})$, respectively. In our case, the function $g(m_{\mbox{\scriptsize elas}})$ is the concatenation of the functions $\mathbf{g}_{\text{scale}}(\mathbf{m}_{\text{elas}}) = \mathbf{m}_{\text{elas lowres}}$ for upscaling the elastic-property model parameter from the high-resolution model to the low-resolution model (at seismic scale) and the forward function calculating the seismic data $\mathbf{g}_{seis}(\mathbf{m}_{elas\ lowers}) = \mathbf{d}_{cal}$. Therefore, the Jacobian of the complete function $\mathbf{g}(\mathbf{m}_{\text{elas}}) = \mathbf{g}_{\text{seis}} \circ \mathbf{g}_{\text{scale}}$ is the product of the corresponding Jacobian matrices $G = G_{\text{scale}}G_{\text{seis}}$, with $G_{\text{scale}} = (\partial m_{\text{elas lowres}} / \partial m_{\text{elas lowres}} / \partial m_{\text{elas loweres}} / \partial m_{\text{e$ $\partial \mathbf{m}_{\text{elas}}$) and $\mathbf{G}_{\text{seis}} = (\partial \mathbf{g}_{\text{seis}} / \partial \mathbf{m}_{\text{elas lowres}})$. The function accounting for the change of scale depends on the specific elastic parameters. In our implementation, we compute the Jacobian matrices by analytical differentiation of the functions involved. The curvature matrix and the steepest-descent direction are derived from the gradient and Hessian of the objective function given by equations 7–9; a description of a similar derivation, for the case of the petrophysical seismic inversion unconditioned to well-log data, is given in Bosch (2004).

SEISMIC, PETROPHYSICAL, AND GEOSTATISTICAL MODELING

Modeling the petrophysical relationships, property geostatistics, and seismic data depends on the setting of the problem. We consider here the case of inverting near-vertical-angle seismic stacked and time-migrated data, which we simulate as zero-offset seismic data reflected in a horizontally layered medium. For each common depth point (CDP), we parameterize the medium in time as a series of homogeneous horizontal layers described by the acoustic impedance as the elastic parameter related with the seismic observations. The seismic signal is modeled by convolving the reflectivity series corresponding to the acoustic impedance model with a source wavelet,

which is estimated at the well-log positions. The choice of acoustic impedance as the physical parameter in the joint model is straightforward from its direct relation, with seismic reflected amplitudes at near-incidence angles.

Model parameters

For modeling the reservoir properties related to acoustic impedance, we describe rock total porosity and pore fluid jointly. Our methods are applied in the setting of a gas reservoir located in clastic strata. No oil is present in the area; the fluid system includes only gas and brine. Hence, the description of the fluid involves only one parameter, which we take as water saturation S_w . Gas saturation is the complement to the unit $S_g = 1 - S_w$ of the water saturation in this case. Our justification for this choice of reservoir parameters is twofold: (1) total porosity and water saturation are properties of major interest for reservoir description and management and (2) both properties strongly relate to acoustic impedance.

We build a petrophysical model to cast these relations, calibrated to the local well-log data. In this application, we do not include rock facies in the property model, which also influences acoustic impedance. We include facies and other effects on acoustic impedance in a random model characterizing the deviations from the petrophysical relationship, based on model porosity and gas saturation. A more complete petrophysical model including facies along with porosity and water saturation is beyond the scope of this work; it would be suggested for the case of inverting multiple angle stack ranges (or multiple offsets) instead of the inversion limited here to the near-vertical-angle data. In this case, improvement in resolution of reservoir properties should result from the information on shear rock behavior embodied in multiangle measurements.

In formulating the geostatistical modeling and inversion, we have made extensive use of Gaussian statistical distributions. Therefore, for the mathematical computations indicated in the previous section, we do not describe porosity and water saturation directly as model parameters. Being bounded properties, they are incompatible with Gaussian assumptions. We transform to the logarithmic porosity ϕ^* = $\ln[\phi/(1-\phi)]$, where ϕ is porosity, and the logarithmic water saturation $S_w^* = \ln[S_w/(1 - S_w)]$, which are unbounded. Inverse transforms are, correspondingly, $\phi = \exp[\phi^*]/(1 + \exp[\phi^*])$ and $S_w = \exp[S_w^*]/(1 + \exp[S_\pi^*])$. The well-log data actually verify that the transforms improve normality of the distribution; further improvement could be obtained with a complementary normalization transform (see Bosch 2004 for a discussion of the logarithmic transform). In summary, our model parameters are the layer acoustic impedance, logarithmic porosity, and logarithmic water saturation, specified at regular time intervals for each CDP: $\mathbf{m}_{\text{elas}} = \{\mathbf{Z}\}$, with \mathbf{Z} being the array specifying layer acoustic impedances, and $\mathbf{m}_{\mathrm{geo}}$ = $\{\phi^*, \mathbf{S}_w^*\}$, with ϕ^* and \mathbf{S}_w^* being the array of logarithmic porosity and logarithmic water saturation.

We fix the impedance low-resolution scale at the limit of the seismic resolution, using 4-ms layers, approximately one-fifth of the dominant period of our seismic data. For the high-resolution time discretization, we use a smaller layer thickness of 1 ms, about 20 times smaller than the dominant period. Hence, we increase the vertical resolution between our two modeled scales a factor of four times. Increasing this factor implies an increase in numerical operations in proportion to the square of the factor for the optimization solution and in proportion to the factor for the Monte Carlo solution. The model resolution in this approach accounts for the significant

layer thickness for practical reservoir description and the size of computations. Therefore, it is fixed between the seismic and the finer well-log resolutions.

Petrophysical model

For the relation between total porosity, water saturation, and acoustic impedance, we model acoustic impedance as a random field conditioned by the total porosity field and water saturation, with a central value that is a deterministic petrophysical transform of porosity and water saturation $\mathbf{f}(\phi^*, \mathbf{S}_w^*)$ plus multivariate Gaussian deviations. We combine two well-known petrophysical relationships to reveal the influence of porosity and water saturation on acoustic impedance. First, we describe the influence of total porosity with a relation straightforwardly derived from the Wyllie time average equation for compressional velocity (Wyllie et al., 1956; Hilterman, 2001) and the corresponding average for density:

$$Z(\phi) = V_{\text{matrix}} \rho_{\text{matrix}} [1 - \phi (1 - \rho_{\text{fluid}} / \rho_{\text{matrix}})] / [1 - \phi]$$

$$\times (1 - V_{\text{matrix}} / V_{\text{fluid}})], \tag{13}$$

with Z being the layer acoustic impedance; ϕ the layer total porosity; and $\rho_{\rm fluid}$, $\rho_{\rm matrix}$, $V_{\rm matrix}$, and $V_{\rm fluid}$ the mass density and compressional velocities for the pure rock matrix and pure fluid, respectively.

Second, we model the fluid compressional velocity with an identity derived from the Wood relation for the bulk modulus (Wood, 1955; Hilterman, 2001) and an identity corresponding to density:

$$\frac{1}{V_{\text{fluid}}^{2}} = \frac{S_{w}^{2}}{V_{\text{brine}}^{2}} + \frac{(1 - S_{w})^{2}}{V_{\text{gas}}^{2}} + S_{w}(1 - S_{w}) \left[\frac{\rho_{\text{gas}}}{\rho_{\text{brine}} V_{\text{brine}}^{2}} + \frac{\rho_{\text{brine}}}{\rho_{\text{gas}} V_{\text{gas}}^{2}} \right].$$
(14)

For fluid density, we have

$$\rho_{\text{fluid}}(S_{\text{W}}) = \rho_{\text{gas}}(1 - S_{\text{W}}) + S_{\text{W}}\rho_{\text{brine}}.$$
 (15)

with $\rho_{\rm gas}$, $\rho_{\rm brine}$, $V_{\rm gas}$, and $V_{\rm brine}$ the gas and brine in situ densities and compressional velocities.

By substituting equations 15 and 14 into equation 13, we obtain our Wyllie-Wood model for the acoustic impedance. We complete our petrophysical transform by making the inverse substitutions of water saturation and porosity in terms of logarithmic water saturation and logarithmic porosity. We use this transform as the deterministic component of the petrophysical model to forward-calculate the acoustic impedance and to calculate the analytical derivatives for the Jacobians in the optimization approach.

Our petrophysical transform is dependent on six parameters — $V_{\rm matrix}, \rho_{\rm matrix}, \rho_{\rm brine}, \rho_{\rm brine}, V_{\rm gas},$ and $\rho_{\rm gas}$ — that characterize the matrix and fluid acoustic behavior. We calibrate these parameters to well-log data in the area by least-squares regression of the well-log impedance estimates and use these values for all of the area. These parameters, however, are actually variable in the area and are affected by other conditions such as the facies. These undetermined effects on acoustic impedance are accounted for in the random component of the petrophysical model $\mathbf{m}_{\rm dev}$.

A final issue on the petrophysical modeling is the change of scale in the impedance, to transform from high-resolution to low-resolution layer discretization. Wave velocities and reflection coefficients O6 Bosch et al.

depend not only on medium properties but also on the frequency content of the signal. Different numerical methods can be used to predict the equivalent elastic properties, given the medium statistical description and frequency content, and simple relationships have been developed for limiting cases. If the wavelength λ is much larger than the typical strata thickness $\lambda \gg d$, we have the common Backus average expressions. In the opposite case, the ray-theory equations hold. However, these two situations are ideal.

Equivalent elastic-medium parameters lie between the two limiting expressions in most practical cases, and different computation methods have been proposed. Some authors (Rio et al., 1996; Grechka, 2003; Stovas and Arntsen, 2006) propose that an average of the two limiting expressions is convenient in many practical situations. Here, we link our high- and low-resolution model scales using an upscaling expression for the impedance:

$$Z_{\text{low res}} = \sqrt{\frac{\sum Z_i}{\sum Z_i^{-1}}},$$
 (16)

with $Z_{\rm low\ res}$ being the equivalent thick-layer acoustic impedance and Z_i the acoustic impedances of the thin layers regularly sampled in traveltime. Expression 16 combines common Backus and mass density depth averages with time conversion in the ray-theory approximation; the results are intermediate between the ray and effective medium formulations.

Geostatistical model and characterization

The third component of information in this work is geostatistical, provided by the well-log constraints to the model parameters. Geostatistical modeling involves several procedures:

- Characterizing the prior mean of the reservoir properties (logarithmic porosity and logarithmic water saturation)
- 2) Characterizing the prior covariance of the reservoir properties
- Calculating the cokriging mean and covariance for the reservoir properties
- Characterizing the prior covariance for the petrophysical misfits (impedance deviation from the petrophysical transform)

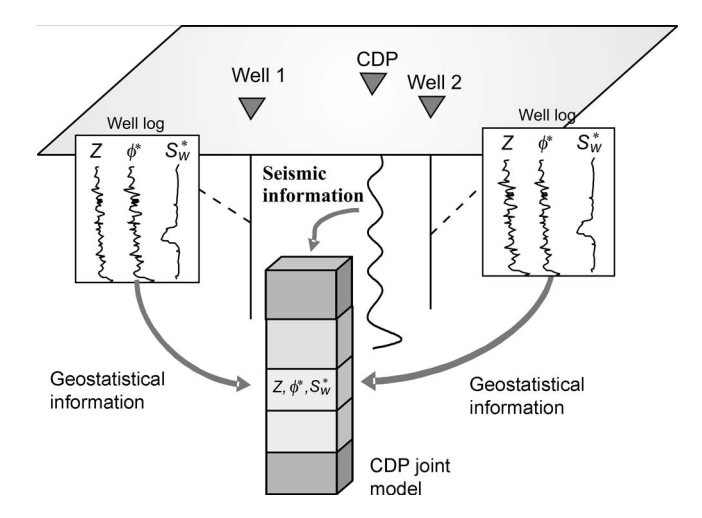


Figure 2. Joint CDP model for acoustic impedance, logarithmic porosity, logarithmic water saturation, information components, and spatial relation with well-log and CDP seismic data.

 Calculating the cokriging mean and covariance for the petrophysical transform deviations

In vertical direction, measured here in time, these covariance functions are modeled from the well-log data. The procedure is illustrated in the following section using field well logs. As is common in geostatistical modeling of reservoirs, we describe lateral covariance between the well data and the properties at the estimation point in reference to structural surfaces previously interpreted from the seismic data to follow the stratification directions.

To produce calculations of reasonable size, we decompose the volume inversion in a set of independent inversions of single CDP joint impedance porosity saturation models. Thus, our inverse problem combines the following information in estimating the 1D impedance porosity saturation model associated with a CDP: (1) well-log data at the surrounding wells, (2) seismic data corresponding to the CDP, and (3) the petrophysical relationship between acoustic impedance, total porosity, and gas saturation. Figure 2 shows the joint 1D model associated with each trace and the information and data involved in the estimation.

MODEL CALIBRATION TO WELL-LOG DATA

We adjust parameters defining the petrophysical and geostatistical models for optimal description of the properties in the area on the basis of well-log-estimated properties, using data from two area well logs. We first upscale the well-log data to high-resolution model discretization (1-ms sampling) via common effective theory expressions and use the upscaled well-log porosity, water saturation, and acoustic impedance to obtain optimal parameters $V_{\rm matrix}$, $P_{\rm matrix}$, $V_{\rm brine}$, $P_{\rm brine}$, $V_{\rm gas}$, and $P_{\rm gas}$ for the Wyllie-Wood petrophysical transform. We achieve this goal by implementing a nonlinear least-squares fitting of the well-log impedance, adapted to the specific transform function.

Figure 3 shows plots of the well-log data points and the corresponding surface defining the petrophysical deterministic Wyllie-Wood transform fitted to the data; Figure 3c is a 3D view of the transform and data points, which correspond to the well-log data used to constrain the inversions in the field case (following). For a closer look into data and model compliance, we show crossplots at particular bands. Our data were clustered in a high-saturation region for brine-saturated rocks and a variable-saturation region at intermediate porosities that corresponded to the gas-reservoir rocks.

Figure 3a shows the fitting of the petrophysical transform for the brine-saturated rocks, including samples with saturation larger than 95%. The gray band shows the size of the standard deviation from the transform used in the statistical model and characterized from the well-log data deviations from the transform predictions. On the other hand, Figure 3b shows a cut of the surface at 30% porosity with the projection of well-log data points within the band from 20% to 40% porosity. The gray band indicates (plus and minus) one standard deviation of the impedance from the predicted petrophysical transform, as characterized and modeled.

To define the parameters of our geostatistical model, we characterized the vertical covariance of the well-log logarithmic porosity and logarithmic water saturation. Figure 4a and b shows the experimental covariance as a function of the time lag, calculated from the well-log estimates for the two properties sampled at 1-ms time intervals, and the corresponding covariance function model fitted to the data. For the covariance function, we used a parametric model mixing basic covariance functions: nugget, Gaussian, and exponential

terms. The corresponding coefficients and parameters of the covariance functions were fitted with a regression procedure to the experimental covariance data. Similarly, we calculated the impedance predicted by the petrophysical transform evaluated at the porosity and saturation well-log data and computed the corresponding deviations from the well-log impedance data.

Figure 4c shows the covariances of the petrophysical relationship data deviations and the corresponding covariance function model. The well-log data show no correlation between water saturation and porosity. Thus, for our synthetic tests and real case, we use zero prior cross-covariances between the two properties.

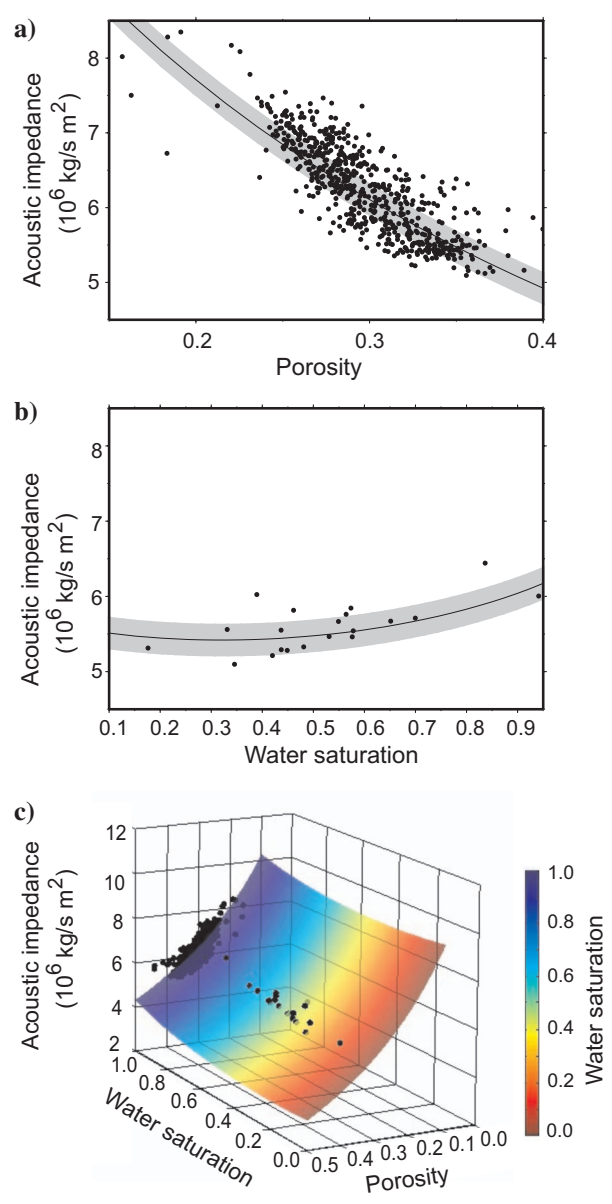


Figure 3. Crossplots of (a) well-log acoustic impedance and water saturation for porosities of (a) 0.95–1.00 and (b) 0.2–0.4. The dark gray line shows the petrophysical transform values after calibration against the well-log data. The clear gray bar shows the size of (plus or minus) one standard deviation of the well-log acoustic impedance from the transform. (c) A 3D view of well-log data (black dots) in acoustic impedance, porosity, and water saturation space and the surface for predicting the acoustic impedance as a function of porosity and water saturation after calibrating the data.

The property covariance in lateral direction is not constrained by the well-log data because wells are vertical in the area. Lateral covariance is subjected to a choice of model and ranges; we use a smooth Gaussian covariance model. As is done for reservoir geostatistical modeling, we use surfaces picked from major seismic continuous events to guide the lateral correlation of the medium properties, ensuring the correlation follows the geometry of the strata. Finally, we build the a 3D property covariance function as the product of the vertical and lateral functions. For more information about covariance function models, see Isaaks and Srivastava (1989) and Chiles and Delfiner (1999).

SYNTHETIC EXAMPLES

We perform numerical tests of the inversion technique using the petrophysical, geostatistical, and seismic source wavelet parameters related to our gas reservoir area. Figure 5 shows a joint total porosity, water saturation, and acoustic impedance model created following artificial structural surfaces and simulated property fields. We locate gas reservoirs in two sand strata as particular targets of the inversion. From the property sections (Figure 5a-c), we calculate the seismic data (Figure 5d), used as observed seismic data for the inversion. Equally, we take the 1D model configuration beneath position 2500 m (X1 in the figure) as observed well logs of acoustic impedance, total porosity, and water saturation to condition the inversion.

For comparison, we present the results of the estimated property fields following three categories of procedures highlighting the in-

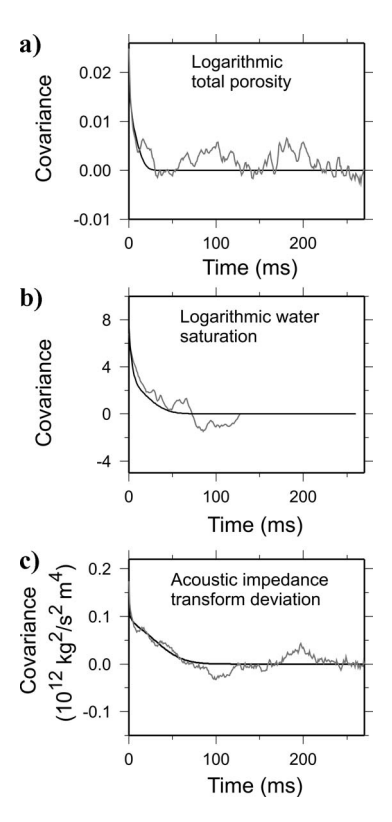


Figure 4. Experimental covariance in time (gray curve) and the corresponding modeled covariance function (solid black curve) for the following well-log-derived properties: (a) logarithmic porosity, (b) logarithmic water saturation, and (c) deviations of well-log-derived acoustic impedance from corresponding values predicted by the petrophysical transform of porosity and water saturation.

O8 Bosch et al.

fluence of each type of information involved in the inference problem:

- Geostatistical estimation from well data, which corresponds to the case of no seismic likelihood information in equation 1. In this case, the result is the cokriging estimate based on the welllog data with covariances, following the structural directions interpreted from the seismic section.
- 2) Petrophysical seismic inversion with no conditioning to well-log data, which corresponds to the case of no well-log spatial constraint to the model. The result combines the information of the seismic data with the petrophysical model relating medium properties. Well-log data are used to build up the global petrophysical and geostatistical models and to extract the source seismic wavelet, but not as spatial constraint to the property fields. As part of the geostatistical model, the expected reservoir properties are given as a linear trend fitted to the well data.

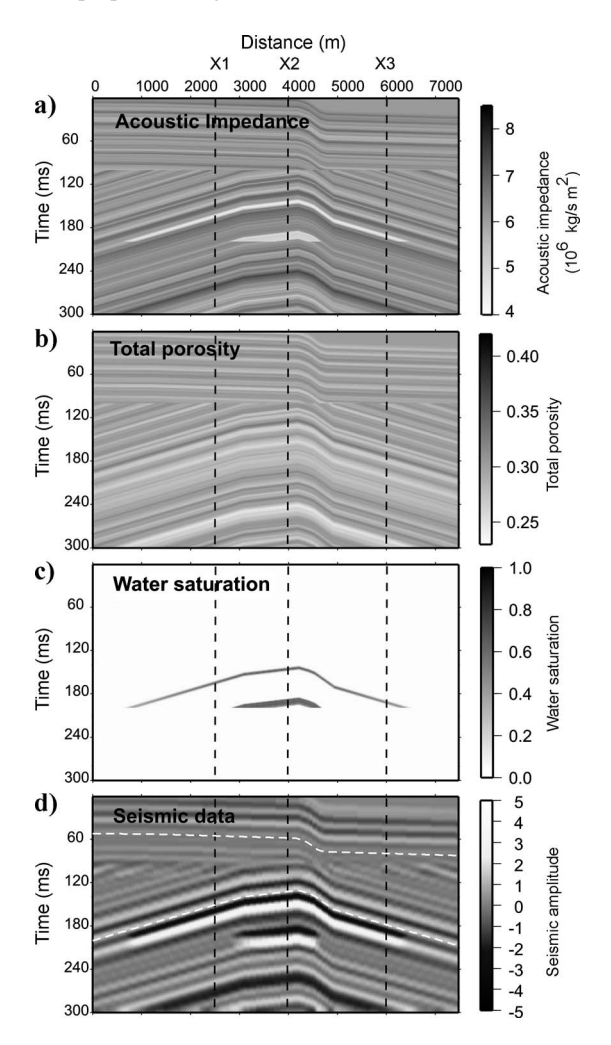


Figure 5. (a) Acoustic impedance, (b) total porosity, and (c) water saturation sections used as true properties for the synthetic tests. (d) The seismic section calculated from the acoustic impedance section and used as observed data for the tests. Location of the virtual well used to condition the inversions is indicated by X1, with the path shown as a black dashed line. Locations X2 and X3 indicate CDP positions used for uncertainty plots in Figure 8, which are also shown as a black dashed line. The two white dashed lines in (d) indicate the polygons used to guide the property covariances along the structure.

 Petrophysical seismic inversion conditioned to well-log data, using the complete formulation described here.

Application of the Monte Carlo inversion technique generates 20,000 model realizations for our synthetic case. We start the sampling chain in the cokriging estimation configuration and perturb the model configurations by combining the geostatistical simulation and the Metropolis sampler as described in a previous section. A typical chi-squared (χ^2) seismic residual plot for a CDP trace located at position X2 indicated in Figure 5 is shown in Figure 6a. In the plot, we distinguish the burn-in phase, influenced by the initial model, and the sampling phase, where model configurations satisfy the seismic observations within uncertainties. With the optimization technique, we initiate the iteration algorithm at the cokriging estimates of the properties and iterate for optimizing jointly the seismic data misfit, petrophysical relationships, and prior geostatistical information. Figure 6b shows a plot of the progress of the χ^2 seismic data misfit, with the iterations of the optimization technique, at the same location X2 of Figure 5.

Figure 7 shows the estimated property fields obtained with the joint seismic and well-log inversion and the two categories based on partial information, solved with the optimization method. Results of the numerical tests show the input of each type of information into the estimated result and the benefit of combining well-log and seismic information. The geostatistical estimation shown in the first column of Figure 7 is based on pure extrapolation of the well-log information, located at the horizontal position of 2500 m, along the strata. We select a 13-km-long range for the lateral covariance along the stratification in these tests. The technique successfully extrapolates the well information following the structural lineation of the strata. However, the second gas reservoir is not predicted in the estimation

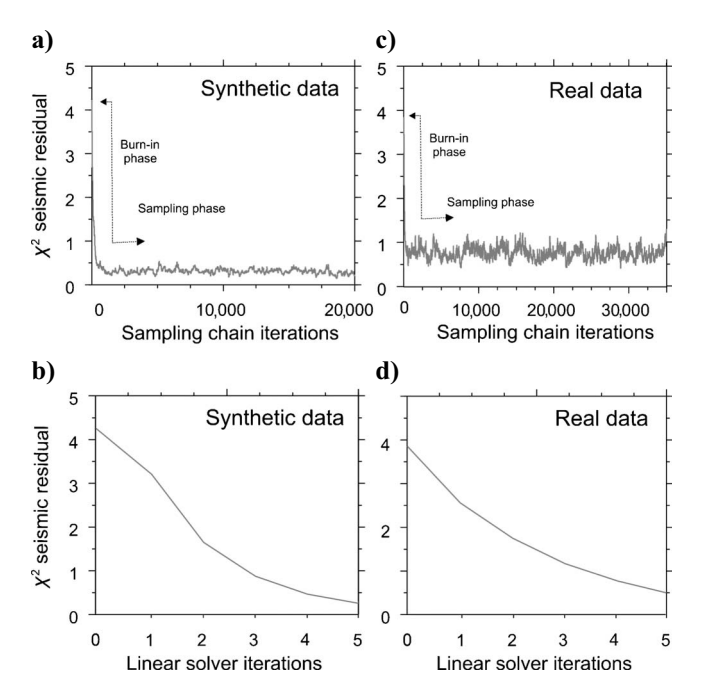


Figure 6. Seismic residual evolution with iterations for the (a) Monte Carlo and (b) optimization algorithms applied to the synthetic data, and the corresponding plots for the (c) Monte Carlo and (d) optimization algorithms applied to the field data. The seismic data residuals are measured in χ^2 . Burn-in and sampling phases are indicated for the Monte Carlo method.

because the true well (path X1 in Figure 5) misses the second gas reservoir. Also, the limits of the first gas reservoir are extrapolated away from the true location. This illustrates that pure geostatistical estimation neglects lateral heterogeneities, as expected.

On the other hand, the seismic petrophysical inversion, shown in the second column, resolves the impedance model at a vertical scale commensurate with the seismic resolution, missing thinner strata present in the target model. Also, because of the coupled effects of porosity and water saturation in the acoustic impedance, the inversion resolves with medium accuracy both reservoir parameters: some features of the porosity stratification are mapped into the water saturation estimation, and vice versa. Nevertheless, the marked decrease of water saturation corresponding to both reservoirs is identified clearly. Also, major stratification of the porosity is correct at seismic scale. Finally, the seismic inversion conditioned to well-log data solves many of the limitations of each type of procedure. As can be seen, each of the properties is better resolved, the two gas reservoirs can be identified, and vertical resolution increases in the region within the lateral covariance range of the well-log data.

Similar results were obtained with the Monte Carlo method. For this method, the estimated fields are the average of the model configurations generated in the sampling phase. As explained earlier, an asset of Monte Carlo sampling is the many model realizations, allowing straightforward estimation of marginal probabilities on model parameters or functions of model parameters. Estimated probabilities correspond to frequencies calculated from the set of model configurations sampled by the chain.

We show in Figure 8a marginal cumulative probabilities for acoustic impedance, total porosity, and water saturation obtained with the petrophysical inversion of seismic data (with no well-log conditioning) at three different distances from the well, corresponding to locations X1, X2, and X3 in Figure 5. Color plots indicate the probability of the property's true value being smaller than or equal to the property axis value, fully describing the uncertainty of the property profiles inferred with the inversion. In our color scale, green plus clear blue areas approximately demark a 0.9 uncertainty bar. The figure also shows the true and estimated property profiles for comparison. Figure 8b is the corresponding probability plots for the petrophysical seismic inversion conditioned to the well-log data at position X1. Comparing this case with the unconditioned inversion, we can verify (1) smaller uncertainties, (2) uncertainties reducing with the distance to the conditioning well log, and (3) higher frequency content in the estimated profiles.

INVERSION RESULTS FOR A GAS RESERVOIR

We apply the inversion method to a stacked and time-migrated small-incidence-angle (within 18° from the vertical) seismic data set in an area of a producing gas reservoir; a section of the seismic data is shown in Figure 9. The area for the inversion corresponds to a clastic sequence with good lateral continuity affected by small faults and mild deformation. As indicated, there is no oil presence in the area; thus, the possible fluids are brine and gas.

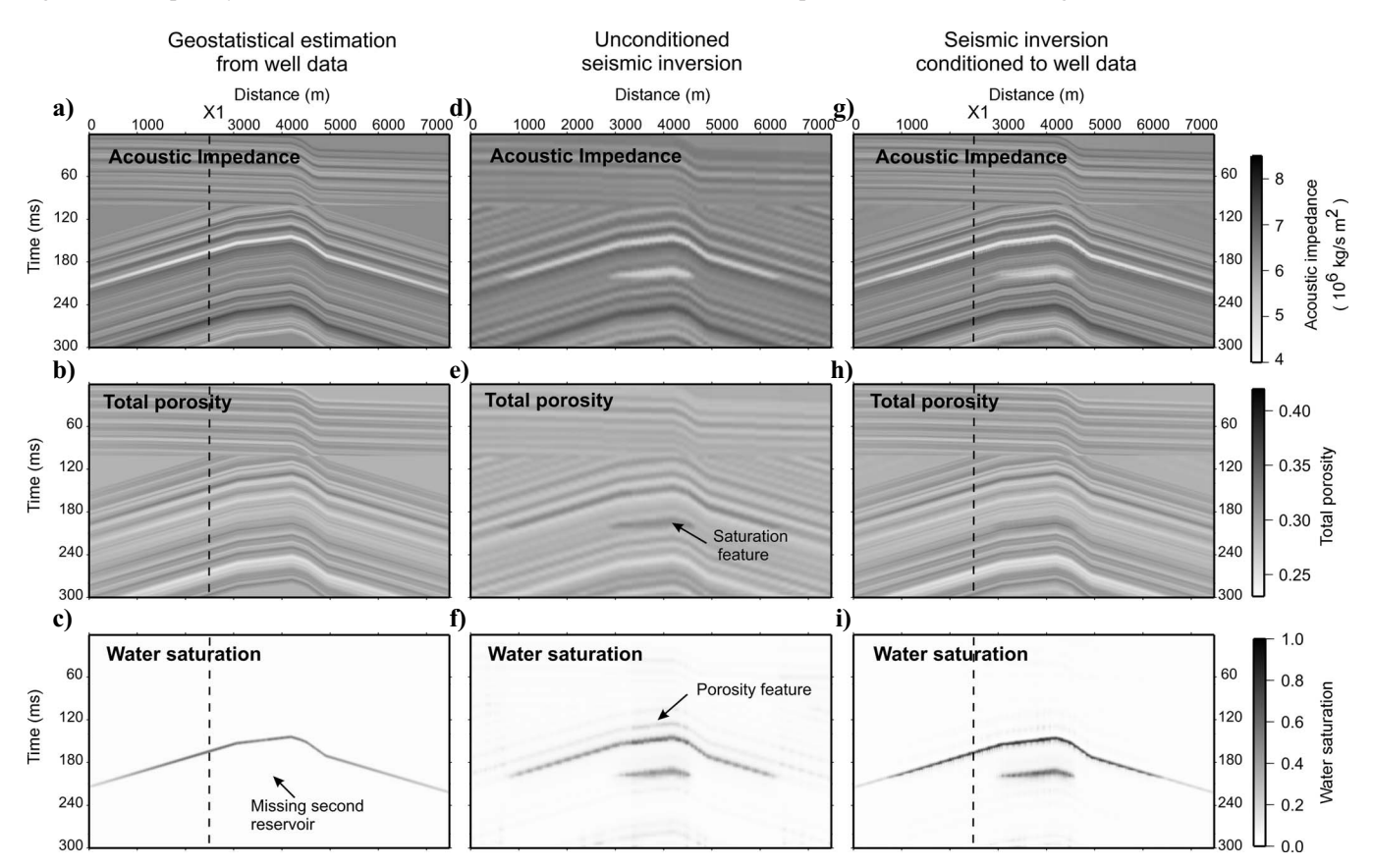


Figure 7. Acoustic impedance, total porosity, and water-saturation sections estimated using the optimization method: (a-c) cokriging true well-log data at well X1, (d-f) petrophysical seismic inversion with no well-log conditioning, and (g-i) joint seismic and well-log-based petrophysical inversion. The conditioning well data are located in the path shown by the black dashed line.

O10 Bosch et al.

We picked a horizon in the seismic section following the major structure of the strata and its small steps to guide the covariance definition. Two wells that intercept the section correspond to the wells and data previously characterized, used to calibrate the petrophysical and geostatistical model. The horizon and position of the two wells are also indicated in Figure 9. Based on the seismic data and well-log-derived impedance, we estimated a source wavelet for the area to simulate the seismic data, similar to a method of Lines and Treitel et al. (1985).

As explained, the 3D covariance function combines the vertical covariance models shown in Figure 4 and a lateral Gaussian covariance model along the reference horizon indicated in Figure 9. Major seismic events show continuity along the reference structural horizon direction for more than 9 km. To account for this continuity, we adopt a lateral covariance range of 13 km to complete the geostatistical model. If a wider area should be treated or major seismic events be less continuous than they are here, the lateral covariance of seismic amplitudes along the structural horizon may be characterized

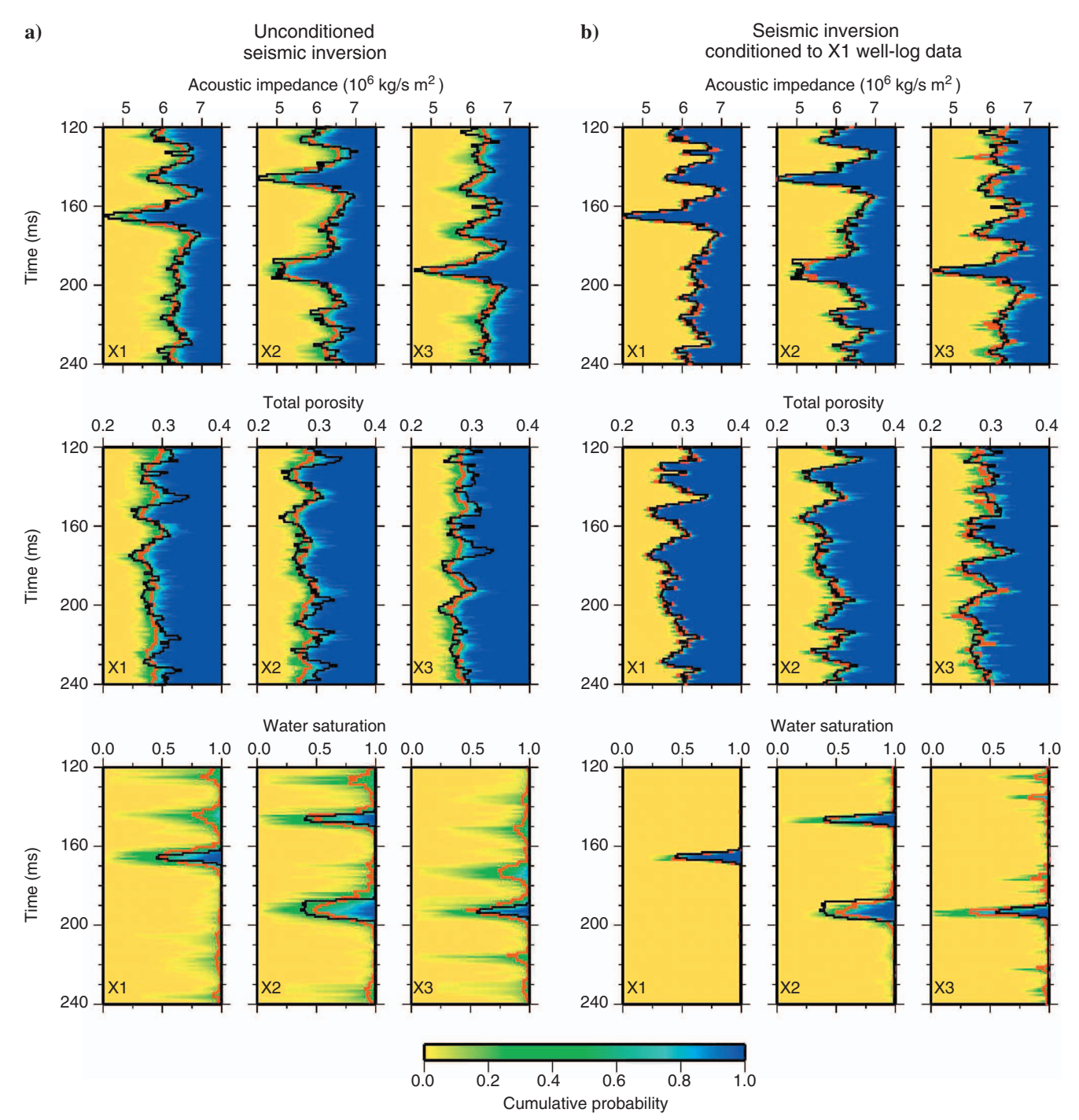


Figure 8. Cumulative marginal probabilities (color plots) calculated from the set of model realizations at CDP locations X1, X2, and X3 (see Figure 5) for (a) unconditioned seismic petrophysical inversion and (b) seismic petrophysical inversion conditioned by well data at X1. The estimated (red lines) and the true (black lines) property profiles are superimposed.

and modeled for constructing the horizontal component of the covariance function, as done for the vertical components in Figure 4.

We present the results of the estimated property fields following the same three procedures categorized for the synthetic tests: (1) geostatistical estimation, (2) petrophysical seismic inversion unconditioned to well-log data, and (3) petrophysical seismic inversion conditioned to well-log data. In these categories, we apply the two solution methods: Monte Carlo sampling and optimization. Parameters defining the petrophysical and geostatistical models are the same for the two solution methods and correspond to the model calibration described previously.

Figure 6c and d shows the progress of seismic data residuals with iterations measured in χ^2 statistic for the CDP model at location X1 (Figure 9). Iterations for the Monte Carlo method (Figure 6c) correspond to steps in the Markov chain associated with perturbations of the model configurations. Estimated fields and probabilities are calculated from the set of realizations generated during the sampling phase of the chain. A similar plot is shown for the optimization approach (Figure 6d), with each iteration corresponding to a model update after constructing and solving the linear system of equations 10-12.

Results with the optimization solution

Property sections obtained with the optimization solution are shown in Figure 10 and correspond to optimal values: maximum combined probability density values obtained by solving equations 10–12 after several iterations, as shown in Figure 6d. The column arrangement of the plots corresponds to the geostatistical solution (cokriging), the seismic inversion with no conditioning to the well-log W1 data, and the seismic inversion conditioned to the well-log W1 data. For all of the plots, the corresponding well-log properties are superimposed at well-path locations of wells W1 and W2 for comparison with the properties estimated with the inversion. Numbers at the bottom of the sections indicate the correlation between the well log and the inversion-estimated properties for each case.

In Figure 10a-c, the geostatistical estimate shows the extrapolation of the conditioning well logs at position W1 along the structural direction; the three properties match the well log at the intersection. Properties progressively tend to the prior mean with increasing distance from the conditioning well log, e.g., the water saturation at the gas reservoir progressively reduces away from well W1. Comparison with the well W2 well-log data shows that major features conveniently have been extrapolated in space because the structure is particularly continuous. However, the geostatistical estimation does not account for the location of medium heterogeneities and the magnitude of property contrasts imprinted on the seismic amplitude information.

For the seismic petrophysical inversion (Figure 10d-f), there is no well constraint; wells are superimposed on the section at their locations W1 and W2 only for comparison with the inversion results. The image shows that the estimated impedance and water saturation have a good match with the corresponding well logs for thick strata, commensurate with the frequency content of the seismic data, as expected; corresponding correlations are shown at the bottom of the plots. The gas saturation looks continuous between the two wells, and no additional gas strata are present, which coincides with independent production information. On the other hand, the low impedance associated with the gas-bearing sand reservoir is mapped partially into the porosity field and water saturation. This results from the common

influence of the two reservoir properties on the acoustic impedance, in this case overestimating the porosity at the site of the reservoir. Also, high well-log porosities that correspond to a shale seal located at approximately 10 ms above the gas reservoir are underestimated. The correlation of the estimated porosity and the well-log porosity is lower than correlations obtained for the other two properties for the unconditional seismic inversion.

The seismic inversion conditioned with the W1 well-log data (Figure 10g-i) improves the match of the estimated properties with both wells (conditioning W1 and blind test W2). Improved correlations are shown at the bottom of the figures for all three model properties — acoustic impedance, water saturation, and total porosity — showing that the well-log information contributes to the resolution across saturation and porosity, which have coupled effects on the acoustic impedance. Also, the plots reveal the increase in the vertical resolution for all estimated property fields where thinner strata have been inferred. The inferred sections are not a plain extrapolation of the W1 well-log data, as in the case of the geostatistical estimation, because they include the medium lateral heterogeneities imprinted in the seismic data. The gas saturation shows continuity along the reservoir.

Results with the Monte Carlo solution

The many realizations produced with the sampling algorithm are used to calculate the estimated fields and probabilities for the three model properties. Figure 8c shows the progress of seismic data residuals and the length of the sampling chain for the real-case application. We used 35,000 iterations of the Monte Carlo sampling algorithm per trace with a burn-in phase of 2000 interations, which provided 33,000 realizations in the sampling phase of the process. The estimated property fields obtained with the Monte Carlo method are similar to the sections shown in Figure 10 estimated with the optimization approach. In addition, by constructing the cumulative frequency of the realizations, we estimated the marginal cumulative probability distribution for each property.

Figure 11a shows the cumulative probability plots for the seismic petrophysical inversion with no well constraints for three CDPs in Figure 9, giving a complete description of the uncertainty associated with the estimate. The color plotted at each point indicates the probability that the property axis value is greater than or equal to the true property value for the corresponding time. Intermediate plot tones between yellow and dark blue can be regarded as marking uncertain-

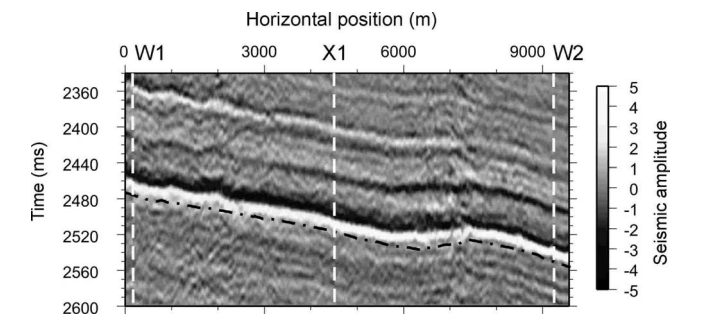


Figure 9. Seismic section that corresponds to a time-migrated stack of small incidence angles ($<\!18^\circ$ from the vertical). Superimposed are the structural horizon used to guide lateral covariances (dot-dashed black line), wells W1 and W2 (dashed line), and an additional location X1 (also dashed white line) used for probability plots in Figure 11.

O12 Bosch et al.

ty bars around the estimated value of the property; the plot zone encompassing the green and clear blue areas approximately corresponds to a 0.9 probability error bar. We superimpose the prior property field, which is a linear trend adjusted to the well-log data, and the inversion-estimated field to the probability plot. Two of the locations correspond to well sites; for comparison, we superimpose the well-log-derived property sampled at 1-ms intervals. Correlations between the well-log and inversion estimates obtained with the Monte Carlo method are shown at the bottom of the plots. Note the appropriate location and magnitude of the water-saturation prediction related to the gas reservoir and the lower frequency content of the seismic inversion result, compared with the well log sampled at 1 ms.

Figure 11b shows the same probability plots corresponding to the results of the seismic petrophysical inversion constrained with well-log data corresponding to well W1. The estimated result and the prior profiles, which in this case correspond to the cokriging estimate, are superimposed; at the conditioning well W1 and the blind test well W2, the well-log-derived properties are also superimposed. We can see from these probability plots that the uncertainty is much smaller at site W1 and increases progressively for sites X1 and W2, as expected.

A few other features are worth mentioning. First, near the conditioning well, the estimated properties closely approximate the well-

log data. Second, our model allows for deviations of the estimated field from the well-log data attributable to the nugget terms modeled in the covariance functions, which implies an amount of independence between the well data and the property field estimated at the nearest CDP. Third, locations and magnitudes of water saturation are adequate at blind test well W2. Fourth, porosity prediction improves from the one corresponding to the unconditioned seismic inversion shown in Figure 11a. Fifth, the vertical resolution of the estimated properties improves. Also, the location and magnitude of the gas saturation at the reservoir level adequately match the well W2 saturation derived from the well-log data.

DISCUSSION

We would like to highlight different assumptions and simplifications made when implementing the method. The petrophysical model is not general purpose and has been developed specifically for gas reservoirs without oil. Different petrophysical models could be implemented, depending on the reservoir situation. Gassmann fluid substitution relations, for instance, could improve the modeling of partial saturation effects on acoustic impedance. A review of common predictive relationships between porosity and compresionalwave velocity, and their combination with Wood's emulsion equa-

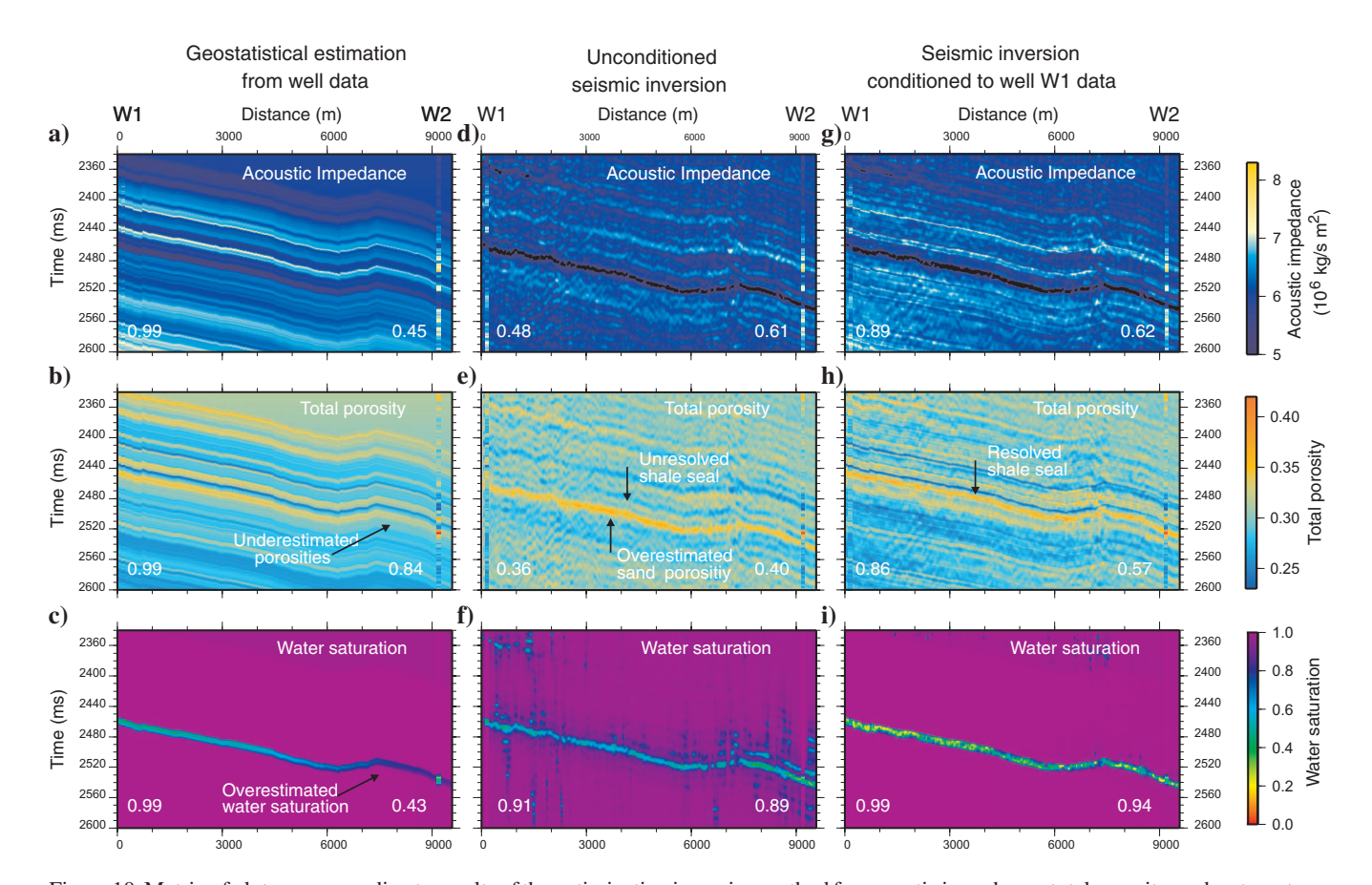


Figure 10. Matrix of plots corresponding to results of the optimization inversion method for acoustic impedance, total porosity, and water saturation. (a-c) Cokriging of well data along the structural horizon. (d-f) Sections estimated by seismic petrophysical inversion with no well-log conditioning. (g-i) Sections estimated by the seismic petrophysical inversion conditioned to well W1 data. At well paths W1 and W2, the well-log-derived properties are superimposed on the corresponding inversion estimates for comparison.

tion, is given in Mavko et al. (2003) and Brereton (1992). With any choice of relationships, validation and calibration of the petrophysical transform with the actual well-log data from the area are needed. Also, more complete petrophysical models can be enhanced to include other parameters, such as facies, to improve deterministic pre-

diction of the elastic parameters. In cases where matrix lithology effects are particularly relevant or fluid-property contrasts are less marked, as in our case, we suggest extending the application to invert multiple offset (or angle) seismic data to estimate a more complete set of reservoir properties.

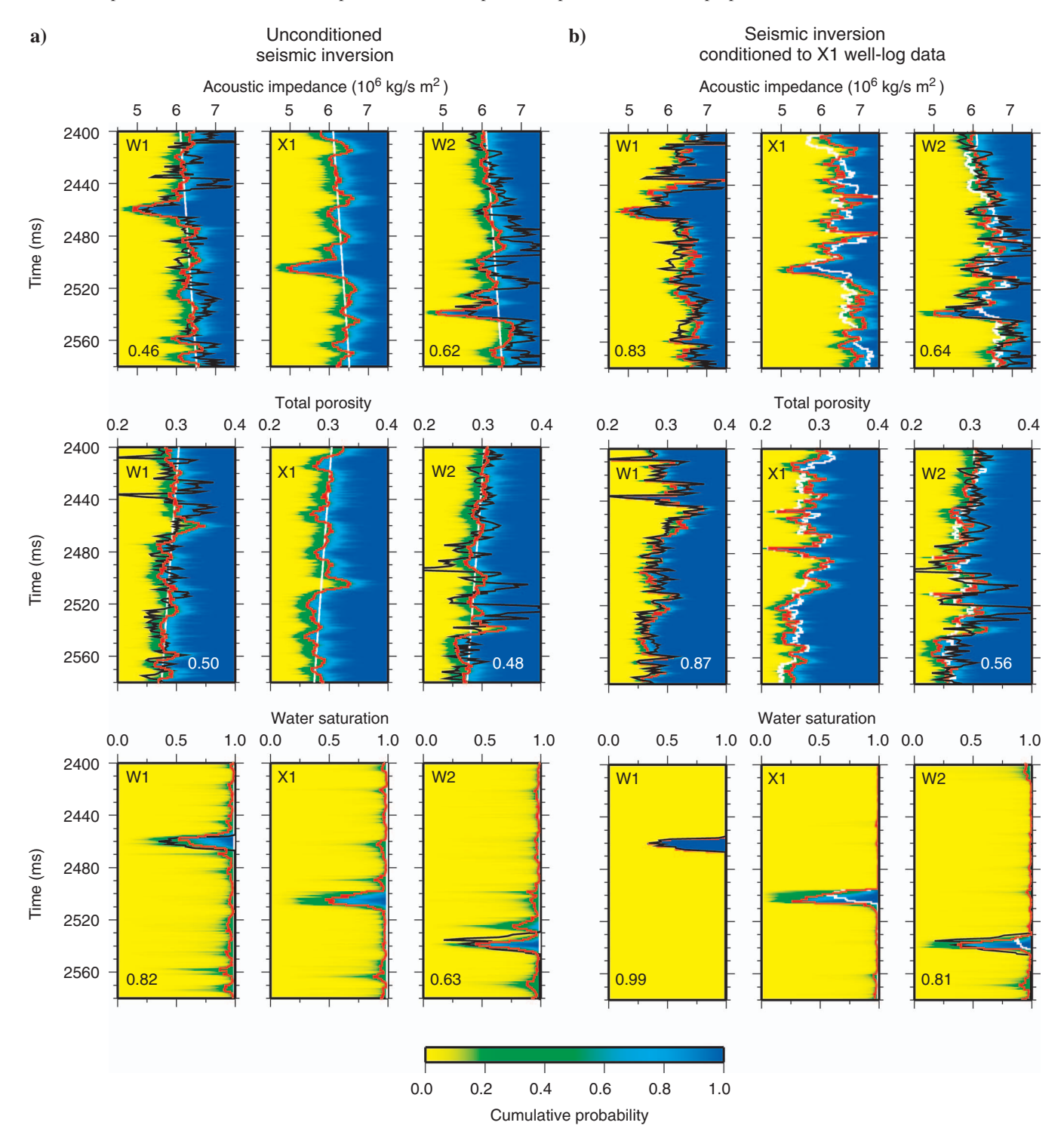


Figure 11. Cumulative marginal probabilities for the model properties (color plots) calculated from the set of joint model realizations for (a) unconditioned seismic petrophysical inversion and (b) seismic petrophysical inversion conditioned to well W1 data shown at CDP locations W1, X1, and W2 (see Figure 9). The estimated property profiles (red lines), the prior property profile (white lines), and the well-log-derived property profiles (black lines) are superimposed.

O14 Bosch et al.

An important advantage of our general petrophysical formulation is that we use a mixed model, combining petrophysical deterministic relationships and random deviations. Well-log statistics may not be representative of the reservoir because of limits on the well numbers or because wells are not drilled randomly. Thus, a purely empirical fit of a function to the well-log data is sensible with poor data coverage. In our model, we use petrophysical relationships calibrated to the well-log data for more robust modeling, consistent with common petrophysical knowledge. On the other hand, none of the deterministic petrophysical transforms fully explains the relation between the variables. Thus, describing well-data deviations from the calibrated relationships allows us to account for the variability of medium properties from these relations.

Upscaling recipes and relationships are a matter of discussion (Lindsay and Van Koughnet, 2001; Liner and Fei, 2007). Well-known situations correspond to the two extremes in wavelength and heterogeneity-size ratios, given by the effective media and ray theories. However, behavior in many common cases is more complicated and involves a combination of the two phenomena. In real cases, we have a distribution of wavelength and medium heterogeneity sizes. In intermediate cases, dispersion and apparent attenuation can be observed, and different approaches have been proposed (Chapman et al., 2006). In our case, the dominant period is approximately 20 times larger than the high-resolution model layer thickness; therefore, rescaling to a seismic resolution layering is required.

We rescale between our low and high model resolution scales directly in the impedance. This is convenient in our formulation because impedance is the elastic parameter in our model, whereas between the original well-log sampling and the high-resolution model scale, we use common effective media expressions. Our upscaling expression for impedance combines ray and effective media considerations and produces results within the two bounds. For the scales we relate in our synthetic and real implementations, our tests with the actual data of the area show that differences are negligible between the effective media average, the ray theory average, and our intermediate model average of the impedance. However, we formulate this issue for generality of the method because it relates the seismic and subseismic scales. In different conditions of model-time sampling, source-frequency composition, or variability of medium properties, the difference in the smoothing approach used for the acoustic impedance could be significant.

Because effects of total porosity and gas saturation in acoustic impedance are coupled, their estimation could be unresolved from the sole information rendered by the near-vertical incidence-angle seismic data. The additional information provided by the nonlinear petrophysical model and the geostatistical characterization of reservoir properties contribute to the resolution of the two properties. However, as shown in the synthetic tests for the unconditioned seismic petrophysical inversion, some features of high gas saturation are mapped partially as high porosities, and vice versa. The coupled effect is given at the level of the petrophysical model because the two properties are uncorrelated at the level of the prior statistical information. Conditioning the inversion to well-log data largely contributes to resolving the ambiguity resulting from the petrophysical coupled effect of the two reservoir properties. On the other hand, plain geostastistical estimation (cokriging) based on the well-log data misses information between the wells carried by the seismic data and related with strata heterogeneities and structural features of major interest in reservoir description. The combination of well-log and seismic inversion builds on the corresponding assets of each type of information to estimate the property fields better.

Another issue of reservoir characterization is the possibility of delineating thin strata. Because of the lateral covariance in the geostatistical model, the high-resolution well-log data extrapolation along the structural directions contributes to the property-field estimates. Joint seismic and well-log inversion improves vertical resolution as a result of the contribution of the well-log data. This is not particularly important for the gas-bearing sand, which has a layer thickness commensurate with the seismic dominant wavelength, but it is clear for other thinner strata. In particular, the acoustic impedance and the porosity sections resolve thin stratification that matches corresponding thin strata at the blind test well W2, located more than 9 km from the conditioning well W1. Correlation is larger and rms deviation is smaller for the joint seismic and well-log-based inversion than for each of the disjoint components for geostatistical and seismic information. Similar results on improving the joint vertical resolution are shown in the synthetic tests.

Because they are based on the same general formulation and assumptions, the results obtained from the Monte Carlo sampling and optimization methods are similar in the method's major features. Minor differences result from particularities of the two-solution approach. Concerning execution times, it is important to notice that the number of iterations shown in Figure 6 for the Monte Carlo and optimization methods cannot be used straightforwardly to compare the associated computation effort. A single iteration of the Monte Carlo method is a very fast process, whereas an iteration of the optimization method requires solving a large system of equations. For the results shown here, the optimization approach is faster by a factor of 20 compared with the Monte Carlo approach for estimating medium properties. However, the Monte Carlo method describes property probabilities (uncertainties) in addition to property estimates.

CONCLUSION

We have developed a general formulation for inverting seismic data under well-log constraints derived from petrophysical and geostatistical models. It allows a joint description and inference of reservoir- and elastic-medium properties. The formulation unifies the steps of geophysical and petrophysical data inversion within a quantitative scheme, accounting for nonlinear relationships, conditioning of estimated property fields to well-log measurements, and combination of uncertainties. We describe solution methods for two major approaches, sampling and optimization, and illustrate the techniques with a synthetic example and an application to field data from a gas reservoir. In this specific setting, we invert seismic near-vertical incidence-angle and well-log data to estimate gas saturation, porosity, and acoustic impedance jointly.

Results of the numerical tests are coherent with the hypotheses of the method. They show that geostatistical interpolation commonly misses laterally discontinuous features, whereas petrophysical seismic inversion (without well conditioning) is limited in frequency according to the seismic signal. Also, the latter is limited in resolving reservoir properties (porosities and saturations), which can be crossmapped partially for some events because of their coupled effect on acoustic impedance. These issues are improved in the petrophysical seismic inversion conditioned with well-log data. In the field case, we base our inference parameters on calibrating the petrophysical transform and the geostatistical characterization of the well logs and transform deviations.

Results of acoustic impedance, water saturation, and porosity jointly honor the seismic data, well logs, and petrophysical model used for the area. We successfully resolve the property fields delineating gas saturation at the level of the reservoir. The seismic petrophysical inversion constrained by well-log data combines assets of the two types of information: increased vertical resolution close to the well, estimated fields that conform to the well logs at intersections, no smoothing of lateral resolution, and adequate joint resolution of water saturation and porosity.

ACKNOWLEDGMENTS

The authors thank CDCH-Universidad Central of Venezuela (PG-08-00-5631-04/08), Petrobras Energía Venezuela, and ENI for their contributions to this research. Also, thanks to the referees and editors for their reviews and comments. This work was done at the Laboratory of Geophysical Simulation and Inversion (LSIG) of the Universidad Central of Venezuela.

REFERENCES

- Bachrach, R., 2006, Joint estimation of porosity and saturation using stochastic rock-physics modeling: Geophysics, 71, no. 5, O53–O63.
- Backus, G. E., 1962, Long-wave elastic anisotropy produced by horizontal layering: Journal of Geophysical Research, **67**, 4427–4440.
- Bosch, M., 1999, Lithologic tomography: From plural geophysical data to lithology estimation: Journal of Geophysical Research, **104**, 749–766.
- ——, 2004, The optimization approach to lithological tomography: Combining seismic data and petrophysical information for porosity prediction: Geophysics, **69**, 1272–1282.
- Bosch, M., L. Cara, J. Rodrigues, A. Navarro, and M. Díaz, 2007, A Monte Carlo approach to the joint estimation of reservoir and elastic parameters from seismic amplitudes: Geophysics, 72, no. 6, O29–O39.
- Brereton, N. R., 1992, Physical property relationships from sites 756 and 766: Proceedings of the Ocean Drilling Program, Scientific Results, 123, 453–468.
- Buland, A., and H. Omre, 2003, Bayesian linearized AVO inversion: Geophysics, 68, 185–198.
- Chapman, M., E. Liu, and X.-Y. Li, 2006, The influence of fluid-sensitive dispersion and attenuation on AVO analysis: Geophysical Journal International, 167, 89–105.
- Chiles, J.-P., and P. Delfiner, 1999, Geostatistics: Modeling spatial uncertainty: John Wiley & Sons, Inc.
- Contreras, A., Č. Torres-Verdin, W. Chesters, and K. Kvien, 2005, Joint stochastic inversion of petrophysical logs and 3D pre-stack seismic data to assess the spatial continuity of fluid units away from wells: Application to a Gulf of Mexico deepwater hydrocarbon reservoir: Transactions of the 46th Annual Logging Symposium, Society of Petrophysicists and Well Log Analysts, Paper UUU.
- Doyen, P. M, 1988, Porosity from seismic data: A geostatistical approach: Geophysics, **53**, 1263–1275.
- Dubrule, O., 2003, Geostatistics for seismic data integration in earth models: SEG.
- Eidsvik, J., P. Avseth, H. More, T. Mukerji, and G. Mavko, 2004, Stochastic

- reservoir characterization using prestack seismic data: Geophysics, **69**, 978–993.
- Geyer, C. J., 1992, Practical Markov chain Monte Carlo: Statistical Science, 7, 473–551.
- Gonzalez, E. F., T. Mukerji, and G. Mavko, 2008, Seismic inversion combining rock physics and multiple-point geostatistics: Geophysics, 73, no. 1, R11–R21.
- Grechka, V., 2003, Effective media: A forward modeling view: Geophysics, 68, 2055–2062.
- Gunning, J., and M. E. Glinsky, 2007, Detection of reservoir quality using Bayesian seismic inversion: Geophysics, **72**, no. 3, R37–R49.
- Haas, A., and O. Dubrule, 1994, Geostatistical inversion—A sequential method of stochastic reservoir modeling constrained by seismic data: First Break, 12, 561–569.
- Hastings, W. K., 1970, Monte Carlo sampling method using Markov chains and their applications: Biometrika, 57, 97–109.
- Hilterman, F. J., 2001, Seismic amplitude interpretation: SEG.
- Isaaks, E., and R. Srivastava, 1989, An introduction to applied geostatistics: Oxford University Press.
- Larsen, A. L., M. Ulvmoen, H. Omre, and A. Buland, 2006, Bayesian lithology/fluid prediction and simulation on the basis of a Markov-chain prior model: Geophysics, 71, no. 5, R69–R78.
- Lindsay, R., and R. Van Koughnet, 2001, Sequential Backus averaging: Upscaling well logs to seismic wavelengths: The Leading Edge, 20, 188–191.
- Liner, C., and T. Fei, 2007, The Backus number: The Leading Edge, **26**, 420–426
- Lines, L., and S. Treitel, 1985, Wavelets, well logs and Wiener filters: First Break, 3, 9–14.
- Mavko, G., T. Mukerji, and J. Dvorkin, 2003, The rock physics handbook: Cambridge University Press.
- Mosegaard, K., and A. Tarantola, 1995, Monte Carlo sampling of solutions to inverse problems: Journal of Geophysical Research, **100**, 12431–12447.
- Mukerji, T., A. Jørstad, P. Avseth, G. Mavko, and J. R. Granli, 2001, Mapping lithofacies and pore-fluid probabilities in a North Sea reservoir: Seismic inversions and statistical rock physics: Geophysics, 66, 988–1001.
- Mukerji, T., G. Mavko, D. Mujica, and N. Lucet, 1995, Scale-dependent seismic velocity in heterogeneous media: Geophysics, 60, 1222–1233.
- Rio, P., T. Mukerji, G. Mavko, and D. Marion, 1996, Velocity dispersion and upscaling in a laboratory-simulated VSP: Geophysics, 61, 584–593.
- Saltzer, R., C. Finn, and O. Burtz, 2005, Predicting V_{shale} and porosity using cascaded seismic and rock physics inversion: The Leading Edge, 24, 732– 736.
- Schoenberg, M., and F. Muir, 1989, A calculus for finely layered anisotropic media: Geophysics, **54**, 581–589.
- Sengupta, M., and R. Bachrach, 2007, Uncertainty in seismic-based pay volume estimation: Analysis using rock physics and Bayesian statistics: The Leading Edge, **24**, 184–189.
- Smith, A. F., and G. O. Roberts, 1993, Bayesian computations via the Gibbs sampler and related Markov chain Monte Carlo methods: Journal of the Royal Statistical Society, 55, 3–23.
- Spikes, K., T. Mukerji, J. Dvorkin, and G. Mavko, 2007, Probabilistic seismic inversion based on rock-physics models: Geophysics, 72, no. 5, R87–R97
- Stovas, A., and B. Arntsen, 2006, Vertical propagation of low-frequency waves in finely layered media: Geophysics, **71**, no. 3, T87–T94.
- Tierney, L., 1994, Markov-chains for exploring posterior distributions: Annals of Statistics, 22, 1702–1762.
- Torres-Verdin, C., M. Victoria, G. Merletti, and J. Pendrel, 1999, Trace-based and geostatistical inversion of 3-D seismic data for thin-sand delineation: An application in San Jorge Basin, Argentina: The Leading Edge, 19, 1070–1077.
- Wood, A. W., 1955, A textbook on sound: Macmillan Publ. Co..
- Wyllie, M. R. J., A. R. Gregory, and L. W. Gardner, 1956, Elastic wave velocities in heterogeneous and porous media: Geophysics, 21, 41–70.